SUPPORTING INFORMATION

A Complementary Chemical and Genomic Screening Approach for Druggable Targets in the Nrf2 Pathway and Small Molecule Inhibitors to Overcome Cancer Cell Drug Resistance

James H. Matthews,[†,‡] Xiao Liang,[†,‡] Valerie J. Paul,[‖] Hendrik Luesch*[,†,‡]

[†]Department of Medicinal Chemistry, [‡]Center for Natural Products, Drug Discovery and Development (CNPD3), University of Florida, Gainesville, Florida 32610, United States

[‖]Smithsonian Marine Station, 701 Seaway Drive, Fort Pierce, Florida 34949, United States

*Corresponding author luesch@cop.ufl.edu

Table of Contents

SUPPLEMENTARY DISCUSSION 3
Potential Mechanisms of Nrf2 Modulation by Cardiac Glycosides 3
Identification of Small Molecule Inducers of Nrf2 Activity 4
Regulation of Nrf2 Activity by Protein Kinase A 4
Potential Mechanisms Underlying the Nrf2 Modulatory Activity of Verified Gene Hits 5
Unique Nrf2 Inhibitory Effects of Lyngbyabellin A and Dolastatin 12 6
METHODS 8
Compound Library Screen 8
Primary ARE-luc screen 8
Secondary ARE-luc screen 8
siRNA library screen 9
Genomic Screen 9
Hit gene validation 9
MDA-MB-231 ARE-luc Reporter Assay 10
Cell Viability Assay 10
RT-qPCR Analysis 10
Immunoblot Analysis 10
Glutathione Content Measurement 11
SUPPLEMENTARY REFERENCES 11
SUPPLEMENTARY FIGURES 16

Supplementary Figures

Figure S1. Representative secondary screen dose-response plots for the putative ARE inhibitors identified in the primary MDA-MB-231 ARE-luc reporter cell line.……16

Figure S2. ARE target gene expression in A549 cells after 24 h exposure to topotecan and mitoxantrone……..17

Figure S3. Combinatorial cytotoxicity assay in A549 cells with stattic and vinblastine ……..…17

Figure S4. 3,4,5,6-tetrahydroxyxanthone activity in MDA-MB-231 ARE-luc reporter cell line.18

Figure S5. Nrf2 inhibitor cytotoxicity in non-tumorigenic cell lines ……...18

Figure S6. Summary of plate statistics from ARE-luc siRNA screen replicates …….……19

Figure S7 siRNA library target gene expression of selected ARE inhibitor hits …….20

Figure S8. Top two enriched networks containing common ARE inhibitor genes hits ……...21

Figure S9. Protein kinase A canonical pathway from Ingenuity Pathway Analysis ……22

Figure S10. Knockdown efficiency of the two independent siRNAs sourced to confirm the five putative ARE inhibitor gene hits in A549 cells...……..23

Figure S11. Dose responses of natural product Nrf2 hits lyngbyabellin A, grassypeptolide A and Dolastatin 12 on A549……...23

Figure S12. Δ Bliss independence calculations for A549 cells co-treated with grassypeptolide A and cisplatin.....……...24

Figure S13. Dose responses of natural product hits lyngbyabellin A, grassypeptolide A and dolastatin 12 on NIH 3T3 cells after 48 h treatment to test cytotoxicity……..…24

Figure S14. Cellular reduced glutathione (GSH) content level did not increase after 24 h natural product Nrf2 inhibitor hits treatment in NIH 3T3 cells……24

Figure S15. Differential ARE inhibitory effect versus cell viability of cytochalasin B and swinholide A from MDA-MB-231 ARE-luc reporter assay…….25

Supplementary Tables

Table S1: Putative ARE inhibitor from the primary compound screen…….26

Table S2: Putative ARE activators from the primary compound screen……...30

Table S3: Enriched networks containing gene hits in common between the two siRNA inhibitor ARE-luc screen replicates……..32

Table S4: Canonical pathway enrichment for the combined ARE inhibitor gene hit list from both siRNA ARE-luc screen replicates…….35

SUPPLEMENTARY DISCUSSION

Potential Mechanisms of Nrf2 Modulation by Cardiac Glycosides

Cardiac glycosides have a long history of therapeutic use, the most common modern application of this class of drugs are in the treatment of congestive heart failure and cardiac arrhythmias. In addition to this application, in recent years there has been renewed interest in the anti-neoplastic activity of cardiac glycosides, many of which display potent cytotoxicity in an array of transformed cell lines. The cellular target of the cardiac glycosides, the Na^+,K^+-ATPase pump, is responsible for maintaining the plasma membrane potential in most cell types and the generation of action potential in neurons[1]. In addition the Na^+,K^+-ATPase pump has been shown to be able to initiate kinase signaling cascades and hence have an intracellular signaling function[2]. Cardiac glycoside binding to the Na^+,K^+-ATPase pump has been shown to cause activation of the tyrosine kinase Src, which in turn activates nearby epidermal growth factor receptor which ultimately leads to activation of the MAPK kinase pathway[3]. Alongside this process, phospholipase C and inositol 1,4,5 triphosphate bridge the gap between the cardiac glycoside bound Na^+,K^+-ATPase pump and the IP3 receptor on the cytoplasmic face of the endoplasmic reticulum membrane causing calcium release and activation of protein kinase C[4]. Given the apparent lack of Nrf2 inhibition by 3,4,5,6-tetrahydroxyxanthone in A549 cells it is possible to speculate that the Nrf2 inhibitory activity of the cardiac glycosides occurs due to their activation of the signaling function of the Na+,K+-ATPase pump, and that Nrf2 inhibition occurs as a consequence of its phosphorylation by a kinase activated via protein kinase C or the MAPK pathway. Inhibition of Nrf2 activity by the cardiac glycosides could also explain the observed increase in cellular ROS after exposure to these compounds[5]. We would postulate that cardiac glycosides bind to the Na^+,K^+-ATPase pump activating the downstream signaling pathway, this decreases Nrf2 activity by direct phosphorylation or phosphorylation of Keap1, which leads to decreased expression of Nrf2 target genes and a rise in basal ROS as a result. Alternatively, the cardiac glycosides may exert their Nrf2 inhibitory activity through their effects on the hypoxia-inducible factor (HIF) pathway. The double deletion of HIF-1α and HIF-2α in HCT116 cells provides a certain degree of resistance to the cytotoxic effects of peruvoside and proscillaridin and cause almost a complete reduction in the cellular levels of the HIF-1α protein[6]. This mechanism would be consistent with the observed effects of ouabain on Nrf2 protein levels in A549 cells (Figure 3d). Given the emerging relationship between the HIF and Nrf2[7] pathways it is possible that the Nrf2 inhibitory effects of the cardiac glycosides are either mediated by the HIF pathway, or are caused by the same upstream events by which HIF-1α levels are depleted.

Identification of Small Molecule Inducers of Nrf2 Activity

While the relatively high basal expression of Nrf2 in MDA-MB-231 cells make them an appropriate cell line with which to identify Nrf2 inhibitors, since Nrf2 is not expressed at maximal levels this cell line should be able identify potential ARE activators. Consistent with this proposition, 33 and 41 putative ARE activators were found in the SIGMA LOPAC and Spectrum Collection library screens, respectively (Figure 2a). These compounds include a number of simple reactive alkylating compounds such as iodoacetamide and carmustine, including those that contain Michael-acceptors such as caffeic acid phenethyl ester (Table S4). However, the majority of the putative ARE inducers are not electrophilic alkylating compounds while it remains to be determined whether these compounds activate Nrf2 by causing the generation of reactive oxygen species, such as with menadione, or by another mechanism. This result highlights the utility of using a reporter cell line with intermediate Nrf2 expression.

Regulation of Nrf2 Activity by Protein Kinase A

The role of protein kinase A in Nrf2 regulation has not been thoroughly explored. However, there is growing evidence that protein kinase A can regulate Nrf2 activity. For example, fasting in mice induces the transcription of ABC transporter genes in the liver under the control of Nrf2, by a mechanism that requires protein kinase A activity[8]. Also, the antioxidant andrographalide was shown to be an adenosine A(2A) receptor agonist that induces heme oxygenase 1 in HepG2 liver cells by a two-fold mechanism in which p38 MAP kinase activation causes up-regulation of Nrf2, and activation of protein kinase A inhibits glycogen synthase kinase 3, which in turn promotes the nuclear retention of Nrf2[9]. While the exact role of protein kinase A activity is unclear in the regulation of Nrf2 activity in cancer cell Nrf2, some of the genes targeted by hit siRNA in this pathway have been previously implicated in Nrf2 activity. For example, *GNA13* encodes guanine nucleotide binding protein 13, whose activity is associated with enhanced cancer cell invasion via its ability to activate Rho kinase. Guanine nucleotide binding protein 13 has been shown to induce Nrf2 activity in mice by regulating the activity of protein kinase C[10]. The enrichment of a large proportion of the canonical pathways was actually driven by protein kinase A and protein kinase C targeting siRNA and reflects the fact that they are counted as components of multiple pathways, as were many of the other siRNA hits (Table S4). This effect is exacerbated by the presence of siRNA that target numerous other multifunctional signaling molecules, the MAP kinases for example.

Potential Mechanisms Underlying the Nrf2 Modulatory Activity of Verified Gene Hits

Twist1 is a basic-helix-loop transcription factor that has contributing role in epithelial-mesenchymal transition and tumor initiation and metastasis, whose activity is regulated by a number of signal transduction pathways including the Akt, MAP kinase, Ras, Wnt and Stat3 pathways, many of which have also been shown to regulate Nrf2 activity[11]. It has been shown that p62/SQSTM1, which is responsible for the autophagic degradation of Keap1, physically interacts with Twist1 and prevents its degradation by the ubiquitin-proteasome system[12]. Furthermore, an *in silico* network analysis of the Nrf2 interactome implicated Twist1 in a miRNA-dependent Nrf2 regulatory mechanism[13]. While the exact mechanism by which Twist1 regulates Nrf2 activity is not clear, and quite likely involves multiple co-regulatory aspects, our results indicate that targeting Twist1 may be a viable strategy for decreasing Nrf2 activity in breast and lung cancer.

Knockdown of another transcription factor encoding gene, *ELF4*[14], also inhibited ARE-luc expression in the MDA-MB-231 reporter cell line and Nrf2 target gene expression in A549 cells. Elf4 is a transcription factor that is highly expressed in peripheral blood and almost every human tissue bar the brain. Despite this near ubiquitous expression, knockout of *ELF4* in mice does not impair embryonic development but does have significant deleterious effects on the functions of T-cells, natural killer cells and natural killer T cells. Elf4 has a complicated role in cancer development and progression and it has been suggested it could act as an oncogene in some cancer types but a tumor suppressor in others*15*. While there is no direct evidence of Elf4 regulating Nrf2, there are hints in the literature of a relationship between these two proteins: (1) The expression of PPAR-γ is positively regulated by Elf4 and Ppar-γ has been shown to regulate *NFE2L2* gene expression; (2) Hif1α transcriptionally activates *ELF4*[14]; (3) An in silico network analysis indicated Elf4 physically interacts with the E3 ubiquitin ligase Skp2, which also interacts with a number of known Nrf2 regulators such as Jak2, Jak3, Myc and Akt1[13]. Our results further implicate a role for Elf4 in regulating Nrf2 activity. The two siRNAs that target the serine/threonine kinase *NEK8* also inhibited ARE-luc expression and Nrf2 target gene expression in A549 cells. Mutations in *NEK8* have been in individuals that suffer from a range of ciliaopathies and mutation of *NEK8* in mice or zebrafish induces a phenotype reminiscient of human autosomal recessive polycystic kidney disease[16, 17]. In *Caenorhabditis elegans*, knockdown of the *NEK8* homologue, nekl-2, by RNAi decreased sodium azide-induced nuclear translocation of the Nrf2 homologue SKN-1 as well as significantly increased their sensitivity to oxidative stress[18]. In humans Nek8 has been implicated in the hippo signal transduction pathway and cell cycle progression

through G_2/M phase. It has been found to be upregulated in breast cancer cells and its downregulation inhibits proliferation of hippo-responsive epithelial and breast cancer cells[19, 20]. Given that knocking down *NEK8* decreases Nrf2 activity, it is possible that part of its anti-profilerative effect of its downregulation could occur via a mechanism that involves reduction of Nrf2 target gene expression.

Tab1 physically interacts with the Tak1 kinase and activates its kinase function[21, 22]. Tak1 is a part of the TGFβ receptor signaling pathway and overexpression of either TAK1 or TAB1 causes activation of the NF-κB signaling pathway. Tak1 has been shown to directly phosphorylate p62/SQSTM1 which enhances its interaction with Keap1, stimulating degradation of Keap1 and hence increasing Nrf2 protein levels, conversely knockdown of TAK1 decreased Nrf2 protein levels by increasing Keap1 protein levels[23]. Our results suggest that Tab1 might be a more attractive target than Tak1, given the challenges in discovering and developing highly specific kinase inhibitors.

Finally, one dual specific phosphatase was verified as a potential Nrf2 inhibitor target, *DUSP4*. Oxidative stress, in the form of H_2O_2, has been shown to induce *DUSP4* gene expression. The subsequent increase in Dusp4 protein levels causes dephosphorylation of JNK following an initial increase in phosphorylated JNK and knockdown of *DUSP4* by siRNA prevents this dephosphorylation[24]. Unsurprisingly, pharmacological activation of Nrf2 also causes an increase in the expression of *DUSP4*, which suggests that *DUSP4* is part of a positive regulatory loop that ensures sustained Nrf2 activity during oxidative stress conditions[25]. Our results suggest that this regulatory loop also exists for the basal activity of Nrf2 in breast and non-small cell lung cancer cells and could be an effective point of intervention at which to decrease Nrf2 activity.

Unique Nrf2 Inhibitory Effects of Lyngbyabellin A and Dolastatin 12

Lyngbyabellin A and dolastatin 12 have both been reported to disrupt the microfilament cytoskeleton by directly interfering with actin polymerization[26-28].Keap1 has been reported to associate with polymerized actin microfilaments in the cytoplasm through its double glycine repeat (DGR or Kelch repeats) domain in NIH3T3 fibroblast cell line[29]. Pharmacological disruption of the actin cytoskeleton has previously been shown to enhance the nuclear import of Nrf2, suggesting a role of the microfilament cytoskeleton in Nrf2-mediated defense pathway. However, in contrast to the results presented herein, exposure of NIH3T3 cells to either actin depolymerization agents cytochalasin B or swinholide A enhanced the nuclear accumulation of an Nrf2 localization reporter

fusion protein and should therefore increase the expression of Nrf2 target genes[29]. We found no evidence that any of the marine natural products tested induce significant cell cytotoxicity (Figure S13) or stimulate glutathione production (Figure S14), a proxy for Nrf2 activation in NIH 3T3 cells, which suggests cell-type and compound specificity for actin targeting compounds and their effect on Nrf2 activity. In addition, to verify the potential of actin disruptors as Nrf2 inhibitors, we tested the Nrf2 inhibitory effects of cytochalasin B and swinholide A using MDA-MB-231 ARE-luc reporter cell line. Interestingly, cytochalasin B did not reduce luciferase activity but mainly caused moderate cell cytotoxicity. In contrast, swinholide A displayed a similar inhibitory window as lyngbyabellin A and dolastatin 12 (Figure S15). Even though cytochalasin B and swinholide A are both reported actin depolymerizing substances, cytochalasin B binds to the barbed of F-actin, inhibits actin elongation and slows filament polymerization, while swinholide A sequesters actin dimers and severs F-actin by interacting with neighboring protomer[30, 31]. Different mechanisms of action of cytochalasin B and swinholide A on actin disruption should account for different outcomes from the MDA-MB-231 ARE-luc reporter assay. Taken the inhibitory effects of lyngbyabellin A and dolastatin 12 on MDA-MB-231 ARE-luc cell line in to consideration, their effects on actin cytoskeleton should be similar to swinholide A rather than cytochalasin B.

METHODS

Compound Library Screen

Primary ARE-luc screen

The MDA-MB-231 ARE-luc reporter cell line was seeded in white 384-well plates at a density of 2.5 x 10^3 cells per well in 50 µl of DMEM medium supplemented with 10% fetal calf serum and 1% Pen/Strep and allowed to attached overnight at 37°C with 5% CO_2 in a humidified incubator. For the primary screen, the SIGMA LOPAC and Spectrum Collection compound libraries were diluted 10-fold in DMSO to create 1 mM dilution plates in 96-well U-bottom polystyrene plates. Compound addition to the 384-well plates was petformed with the Janus MDT Workstation (Perkin-Elmer) using a slotted pin tool capable of delivering ~0.5 µL per well to give a final concentration of 10 µM. Compounds were screened in quadruplicate and each 384-well plate contained 16 positive control ARE inhibitor wells with 125 nM brusatol and 16 negative control wells with 0.5% DMSO. After compound addition the 384-well plates were incubated for 24 h at 37°C with 5% CO2 in a humidified incubator after which ARE-luc expression was quantified using the BriteLite reagent (Perkin-Elmer). The BriteLite reagent was prepared according to the manufacterers instrcutions and diluted two-fold with MilliQ filtered water and 50 µL of the diluted reagent was added per well after the 384-well plates had been allowed to reach room temperature. After incubation for 5 min at room temperature luminescence was quantified using the EnVision Multilabel Plate Reader fitted with a 384-well plate fitted with a 384-well in Ultra Sensitive luminescence mode. The raw luminescence reading for each well was standardized by dividing by the median luminescence for each plate. Standardized well luminescence was used to calculate the median absolute deviation (MAD) score of each well and the average MAD score for each quadruplicate treatment was calculated. A hit compound was defined as one with an average MAD score less than 50% of the average negative control MAD score.

Secondary ARE-luc screen

Selected primary screen hits were assayed in the same manner as the primary screen using compound source plates that contained 7-point, two-fold serial dilution series of each compound in DMSO starting at 1 mM. Each serial dilution plate was added to two replicate 384-well plates, one of which was used to quantify ARE-luc expression as above. The second plate was used to quantify cell viability using the CellTiter 96 Non-radioactive Cell Proliferation (MTT) assay

(Promega) according to the manufacturer's instructions on the SpectraMax plate reader (Molecular Devices) with 150 ms exposure time.

siRNA library screen

Genomic Screen

The Druggable Genome Library V3.0 siRNA library (Ambion) was screened by reverse transfection in the MDA-MB-231 ARE-luc reporter cell line using the protocol previously reported6. In brief, the siRNA was spotted into white opaque 384 well plates using the HydraDT liquid handling robot (Matrix Technologies Corporation) to give a final concentration of 20 nM after media addition. Opti-MEM reduced serum medium containing siLentFect transfection reagent (BioRad) was added to each plate, 20 µL per well, and incubated for 20 min at room temperature. The MDA-MB-231 ARE-luc reporter cell line was dispensed into each well, to give 1.5 x 10^3 cell/s per well, in 20 µL of DMEM medium supplemented with 20% fetal calf serum. Plates were incubated at 37°C in a humidified incubator with 5% CO_2 for 72h. ARE-luc expression and cell viability was quantified in same manner as for the compound library screens 72 h post-transfection. Each 384-well plate contained 16 negative control wells containing Silencer Negative Control No. 1 siRNA (Ambion) and 16 positive control wells containing 50 nM SMARTpool siRNA targeting NFE2L2 (Dharmacon). The online CARD web application[32] was used to standardize the luminescence output from each well to the average of the negative control wells. An individual siRNA hit was defined as one that caused greater than 50% reduction of response compared to the negative control. A hit gene in each screen was defined as one that was targeted by two or more hit siRNA.

Hit gene validation

Hit genes were confirmed by testing the effect of two independent, previously validated, siRNA per gene on the expression of the ARE-luc reporter in MDA-MB-231 cells. Duplicate 96-well white plates were seeded with 2.5 x 10^3 cells per well in DMEM medium supplemented with 10% FCS and 1% Pen/Strep and allowed to attach overnight. Medium was removed and replaced with 50 µL of DMEM medium supplemented with 20% FCS one hour prior to the addition of 50 µL of OptiMEM medium containing a two-fold serially diluted series of siRNA-siLentFect transfection reagent (Bio-Rad) complexes to give a final concentration range of 100 nM to ~1.5 nM. After 72 h incubation ARE-luc expression was quantified in one plate using the BriteLite reagent and cell viability was quantified in the remaining plate using the ATPLite Plus reagent.

MDA-MB-231 ARE-luc Reporter Assay

MDA-MB-231 ARE-luc cells (10,000 cells/well) were seeded in 96-well plates and treated with serial dilutions of individual compounds or solvent control the next day for 24 h. ARE activities were detected using BriteLite detection reagent (PerkinElmer). Each condition was tested in triplicate.

Cell Viability Assay

MDA-MB-231 or A549 cells were seeded in 96-well plates at the density of 10,000 cells/well. The next day, cells were treated with serial dilutions of individual compounds or solvent control for 24 h. the cell viability was assessed using a MTT cell proliferation assay according to the manufacturer's instructions (Promega). Each condition was tested in triplicate.

RT-qPCR Analysis

MDA-MB-231 or A549 cells were seeded in 6-well plates at a density of 200,000 cells per well and treated with individual compounds or solvent control the next day for 24 h. The treatment concentrations were selected based on reporter assay screening results, in which the cell ARE inhibitory activity is about 80% which cell viability still maintains at more than 70%. Total RNA was extracted with RNeasy Mini Kit (Qiagen) and the concentration of RNA was measured using NanoDrop 2000 Spectrophotometer (Thermo Fisher Scientific). Following cDNA synthesis was from 2 μg total RNA by using Oligo(dT) 12-18 Primer (Invitrogen) and SuperScript II Reverse Transcriptase (Invitrogen). Real-time PCR was performed with the ABI 7300 sequence detection system (Applied Biosystems). Each assay was carried out in triplicate. The expression of GAPDH was used as endogenous control for normalization.

Immunoblot Analysis

A549 cells were seeded in 6-well plates (200,000 cells/well) and treated with compound or solvent the next day for 24 h. After treatment, the whole cell lysates were collected using PhosphoSafe buffer (EMD Chemicals, Inc.). Protein concentrations were quantified with BCA Protein Assay kit (Thermo Fisher Scientific). Equal amounts of protein were separated by SDS-PAGE gel electrophoresis (NuPAGE Novex 4-12% Bis-Tris Mini gels, Invitrogen) first, followed by being transferred to PVDF membranes. The membranes were probed with primary

and secondary antibodies and visualized using Li-Cor imaging system. Anti-GAPDH and anti-NQO1 antibodies were obtained from Invitrogen. Secondary anti-mouse and anti-rabbit antibodies were from Invitrogen as well.

Glutathione Content Measurement

Glutathione assays were performed following the manufacturer's instructions. A549 cells were seeded into 6-well plates (800,000 cells/well) and incubated at 37 °C overnight before treatment. The cells were treated with compound hits with indicated concentrations for 24 h at 37 °C before deproteinization. The cells were washed twice with DPBS and harvested before deproteinized in 3 volumes of 5% sulfosalicylic acid solution (v/v, SSA). The resulted suspension was frozen in liquid nitrogen and thawed in 37 °C water bath twice and incubated at 4 °C for 5 min. The cell debris was then centrifuged at 10,000 x g for 10 min at 4 °C. The supernatant was used as glutathione stock for following measurement. The concentration of the total glutathione (GSH+GSSG) was determined by comparing with a standard curve of reduced glutathione (GSH).

SUPPLEMENTARY REFERENCES

[1] Prassas, I., and Diamandis, E. P. (2008) Novel therapeutic applications of cardiac glycosides, *Nat. Rev. Drug Discov. 7*, 926-935.

[2] Cui, X. Y., and Xie, Z. J. (2017) Protein Interaction and Na/K-ATPase-Mediated Signal Transduction, *Molecules 22*, E990

[3] Liang, M., Cai, T., Tian, J., Qu, W. K., and Xie, Z. J. (2006) Functional characterization of Src-interacting Na/K-ATPase using RNA interference assay, *J. Biol. Chem. 281*, 19709-19719.

[4] Yuan, Z. K., Cai, T., Tian, J., Ivanov, A. V., Giovannucci, D. R., and Xie, Z. J. (2005) Na/K-ATPase tethers phospholipase C and IP3 receptor into a calcium-regulatory complex, *Mol. Biol. Cell 16*, 4034-4045.

[5] Xie, Z. J., Kometiani, P., Liu, J., Li, J., Shapiro, J. I., and Askari, A. (1999) Intracellular reactive oxygen species mediate the linkage of Na+/K+-ATPase to hypertrophy and its marker genes in cardiac myocytes, *J. Biol. Chem. 274*, 19323-19328.

[6] Bousquet, M. S., Ma, J. J., Ratnayake, R., Havre, P. A., Yao, J., Dang, N. H., Paul, V. J., Carney, T. J., Dang, L. H., and Luesch, H. (2016) Multidimensional Screening Platform for Simultaneously Targeting Oncogenic KRAS and Hypoxia-Inducible Factors Pathways in Colorectal Cancer, *ACS Chem. Biol. 11*, 1322-1331.

[7] Toth, R. K., and Warfel, N. A. (2017) Strange Bedfellows: Nuclear Factor, Erythroid 2-Like 2 (Nrf2) and Hypoxia-Inducible Factor 1 (HIF-1) in Tumor Hypoxia, *Antioxidants 6*, pii: E27

[8] Kulkarni, S. R., Donepudi, A. C., Xu, J. L., Wei, W., Cheng, Q. Q. C., Driscoll, M. V., Johnson, D. A., Johnson, J. A., Li, X. L., and Slitt, A. L. (2014) Fasting Induces Nuclear Factor E2-Related Factor 2 and ATP-Binding Cassette Transporters via Protein Kinase A and Sirtuin-1 in Mouse and Human, *Antioxid. Redox Sign. 20*, 15-30.

[9] Mittal, S. P. K., Khole, S., Jagadish, N., Ghosh, D., Gadgil, V., Sinkar, V., and Ghaskadbi, S. S. (2016) Andrographolide protects liver cells from H2O2 induced cell death by upregulation of Nrf-2/HO-1 mediated via adenosine A(2a) receptor signaling, *BBA-Gen. Subjects 1860*, 2377-2390.

[10] Cho, M. K., Kim, W. D., Ki, S. H., Hwang, J. I., Choi, S., Lee, C. H., and Kim, S. G. (2007) Role of G alpha(12) and g alpha(13) as novel switches for the activity of Nrf2, a key antioxidative transcription factor, *Mol. Cell. Biol. 27*, 6195-6208.

[11] Zhao, Z. X., Rahman, M. A., Chen, Z. G., and Shin, D. M. (2017) Multiple biological functions of Twist1 in various cancers, *Oncotarget 8*, 20380-20393.

[12] Qiang, L., Zhao, B. Z., Ming, M., Wang, N., He, T. C., Hwang, S., Thorburn, A., and He, Y. (2014) Regulation of cell proliferation and migration by p62 through stabilization of Twist1, *P. Natl. Acad. Sci. USA 111*, 9241-9246.

[13] Turei, D., Papp, D., Fazekas, D., Foldvari-Nagy, L., Modos, D., Lenti, K., Csermely, P., and Korcsmaros, T. (2013) NRF2-ome: An Integrated Web Resource to Discover Protein Interaction and Regulatory Networks of NRF2, *Oxid. Med. Cell Longev. 2013*, 737591.

[14] Suico, M. A., Shuto, T., and Kai, H. (2017) Roles and regulations of the ETS transcription factor ELF4/MEF, *J. Mol. Cell Biol. 9*, 168-177.

[15] Sashida, G., Bazzoli, E., Menendez, S., Liu, Y., and Nimer, S. D. (2010) The oncogenic role of the ETS transcription factors MEF and ERG, *Cell Cycle 9*, 3457-3459.

[16] Liu, S. M., Lu, W. N., Obara, T., Kuida, S., Lehoczky, J., Dewar, K., Drummond, I. A., and Beier, D. R. (2002) A defect in a novel Nek-family kinase causes cystic kidney disease in the mouse and in zebrafish, *Development 129*, 5839-5846.

[17] Frank, V., Habbig, S., Bartram, M. P., Eisenberger, T., Veenstra-Knol, H. E., Decker, C., Boorsma, R. A. C., Gobel, H., Nurnberg, G., Griessmann, A., Franke, M., Borgal, L., Kohli, P., Volker, L. A., Dotsch, J., Nurnberg, P., Benzing, T., Bolz, H. J., Johnson, C., Gerkes, E. H., Schermer, B., and Bergmann, C. (2013) Mutations in NEK8 link multiple organ dysplasia with altered Hippo signalling and increased c-MYC expression, *Hum. Mol. Gen. 22*, 2177-2185.

[18] Kell, A., Ventura, N., Kahn, N., and Johnson, T. E. (2007) Activation of SKN-1 by novel kinases in *Caenorhabditis elegans*, *Free Radic. Biol. Med. 43*, 1560-1566.

[19] Bowers, A. J., and Boylan, J. F. (2004) Nek8, a NIMA family kinase member, is overexpressed in primary human breast tumors, *Gene 328*, 135-142.

[20] Habbig, S., Bartram, M. P., Sagmuller, J. G., Griessmann, A., Franke, M., Muller, R. U., Schwarz, R., Hoehne, M., Bergmann, C., Tessmer, C., Reinhardt, H. C., Burst, V., Benzing, T., and Schermer, B. (2012) The ciliopathy disease protein NPHP9 promotes nuclear delivery and activation of the oncogenic transcriptional regulator TAZ, *Hum. Mol. Gen. 21*, 5528-5538.

[21] Shibuya, H., Yamaguchi, K., Shirakabe, K., Tonegawa, A., Gotoh, Y., Ueno, N., Irie, K., Nishida, E., and Matsumoto, K. (1996) TAB1: An activator of the TAK1 MAPKKK in TGF-beta signal transduction, *Science 272*, 1179-1182.

[22] Sakurai, H., Miyoshi, H., Toriumi, W., and Sugita, T. (1999) Functional interactions of transforming growth factor beta-activated kinase 1 with I kappa B kinases to stimulate NF-kappa B activation, *J. Biol. Chem. 274*, 10641-10648.

[23] Hashimoto, K., Simmons, A. N., Kajino-Sakamoto, R., Tsuji, Y., and Ninomiya-Tsuji, J. (2016) TAK1 Regulates the Nrf2 Antioxidant System Through Modulating p62/SQSTM1, *Antiox. Redox Signal. 25*, 953-964.

[24] Barajas-Espinosa, A., Basye, A., Angelos, M. G., and Chen, C. A. (2015) Modulation of p38 kinase by *DUSP4* is important in regulating cardiovascular function under oxidative stress, Free *Radic. Biol. Med. 89*, 170-181.

[25] Yates, M. S., Tran, Q. T., Dolan, P. M., Osburn, W. O., Shin, S., McCulloch, C. C., Silkworth, J. B., Taguchi, K., Yamamoto, M., Williams, C. R., Liby, K. T., Sporn, M. B., Sutter, T. R., and Kensler, T. W. (2009) Genetic versus chemoprotective activation of Nrf2 signaling: overlapping yet distinct gene expression profiles between Keap1 knockout and triterpenoid-treated mice, *Carcinogenesis 30*, 1024-1031.

[26] Tan, L. T. (2010) Filamentous tropical marine cyanobacteria: a rich source of natural products for anticancer drug discovery, *J. Appl. Phycol. 22*, 659-676.

[27] Luesch, H., Yoshida, W. Y., Moore, R. E., Paul, V. J., and Mooberry, S. L. (2000) Isolation, structure determination, and biological activity of lyngbyabellin A from the marine cyanobacterium *Lyngbya majuscula*, *J. Nat. Prod. 63*, 611-615.

[28] Harrigan, G. G., Yoshida, W. Y., Moore, R. E., Nagle, D. G., Park, P. U., Biggs, J., Paul, V. J., Mooberry, S. L., Corbett, T. H., and Valeriote, F. A. (1998) Isolation, structure determination, and biological activity of dolastatin 12 and lyngbyastatin 1 from *Lyngbya majuscula*/*Schizothrix calcicola* cyanobacterial assemblages, *J. Nat. Prod. 61*, 1221-1225.

[29] Kang, M. I., Kobayashi, A., Wakabayashi, N., Kim, S. G., and Yamamoto, M. (2004) Scaffolding of Keap1 to the actin cytoskeleton controls the function of Nrf2 as key regulator of cytoprotective phase 2 genes, *Proc. Natl. Acad. Sci. USA 101*, 2046-2051.

[30] Holzinger, A., and Blaas, K. (2016) Actin-Dynamics in Plant Cells: The Function of Actin-Perturbing Substances: Jasplakinolide, Chondramides, Phalloidin, Cytochalasins, and Latrunculins, *Methods Mol. Biol. 1365*, 243-261.

[31] Bubb, M. R., Spector, I., Bershadsky, A. D., and Korn, E. D. (1995) Swinholide A is a microfilament disrupting marine toxin that stabilizes actin dimers and severs actin filaments, *J. Biol. Chem. 270*, 3463-3466.

[32] Dutta, B., Azhir, A., Merino, L. H., Guo, Y. J., Revanur, S., Madhamshettiwar, P. B., Germain, R. N., Smith, J. A., Simpson, K. J., Martin, S. E., Beuhler, E., and Fraser, I. D. C.

(2016) An interactive web-based application for Comprehensive Analysis of RNAi-screen Data, *Nat. Comm. 7*. 10578.

SUPPLEMENTARY FIGURES

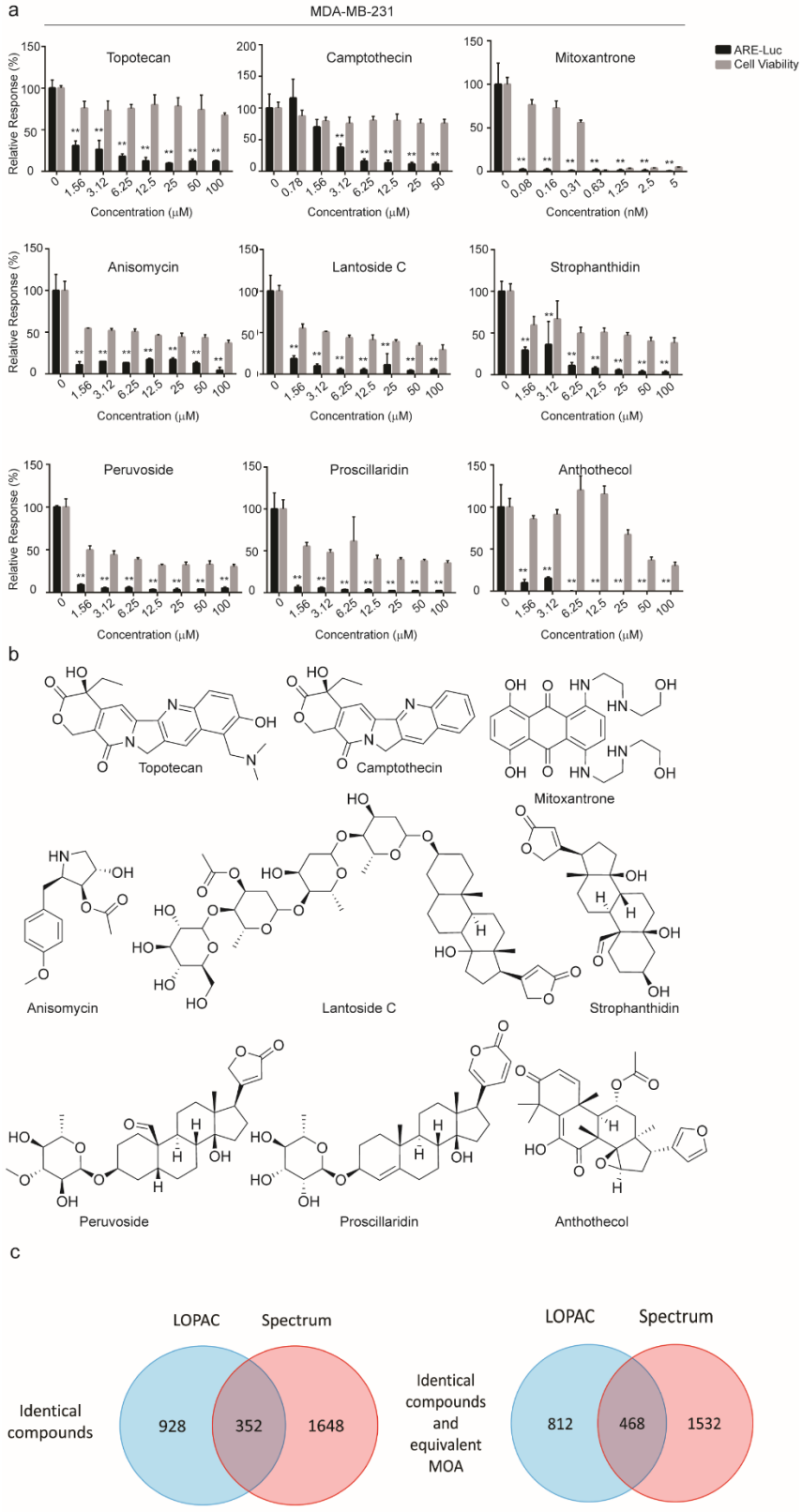

Figure S1. a) Representative secondary screen dose-response plots for the putative ARE inhibitors identified in the primary MDA-MB-231 ARE-luc reporter cell line. ARE-luc expression was quantified using the BriteLite reagent (Perkin-Elmer) and cell viability was quantified with the

CellTiter 96 Non-radioactive Cell Proliferation (MTT) assay (Promega) after 24 h. **b)** Putative ARE inhibitor structures. **c)** Venn diagram depicting compound library overlap of identical compounds and compounds with equivalent mechanisms. Error bars represent ± SEM, ** P ≤ 0.01 (One way ANOVA) relative to negative control.

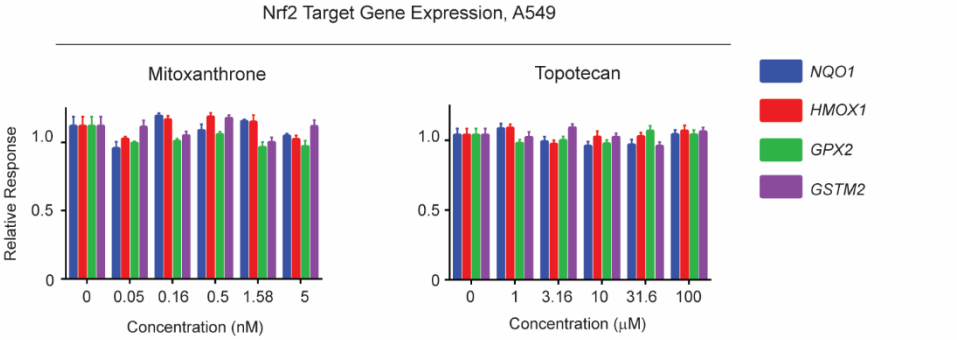

Figure S2. ARE target gene expression in A549 cells after 24 h exposure to topotecan and mitoxantrone. The expression of four Nrf2 target genes (*NQO1*, *HMOX1*, *GPX2* and *GSTM2*) was quantified by RT-qPCR using *GAPDH* as the reference gene. Error bars represent ± SEM.

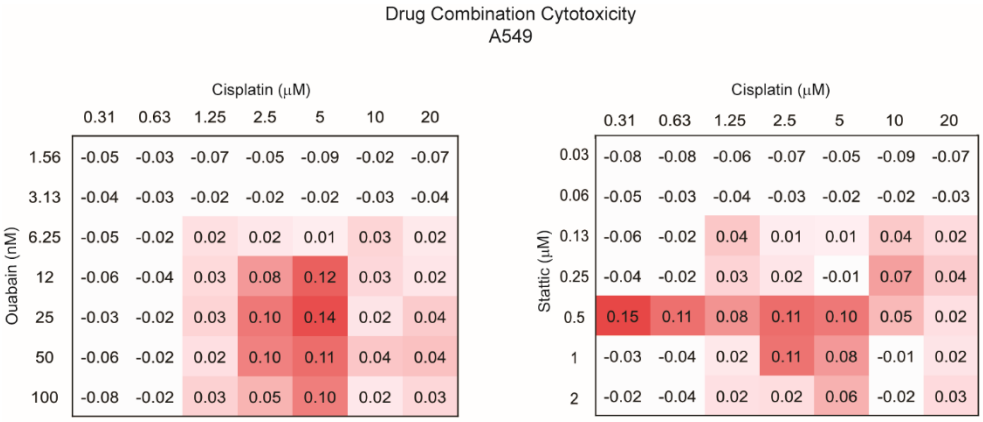

Figure S3. *In vitro* A549 cell combination cytotoxicity assay. A549 cells were pre-treated for 6 h with the indicated concentrations of ouabain or stattic before the addition of cisplatin. Viability was quantified using the MTT assay after a total of 72 h drug exposure and expressed relative to the negative control (0.5% DMSO). Error bars represent ± SEM.

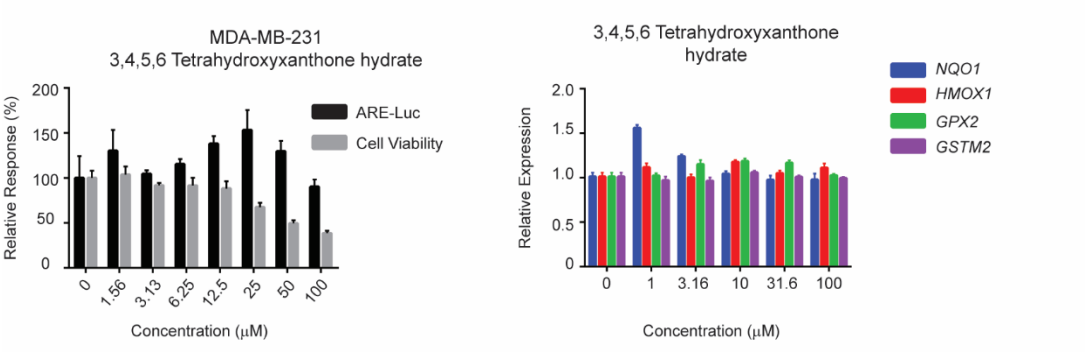

Figure S4. ARE-luc activity in MDA-MB-231 cells and Nrf2 target gene expression in A549 cells after 24 h exposure to 3, 4, 5, 6 tetrahydroxyxanthone hydrate. Luciferase activity was measured using the BriteLite reagent and cytotoxicity was assessed with the MTT assay after 24 h drug exposure. The expression of four Nrf2 target genes (*NQO1*, *HMOX1*, *GPX2* and *GSTM2*) was quantified by RT-qPCR using *GAPDH* as the reference gene. Error bars represent ± SEM.

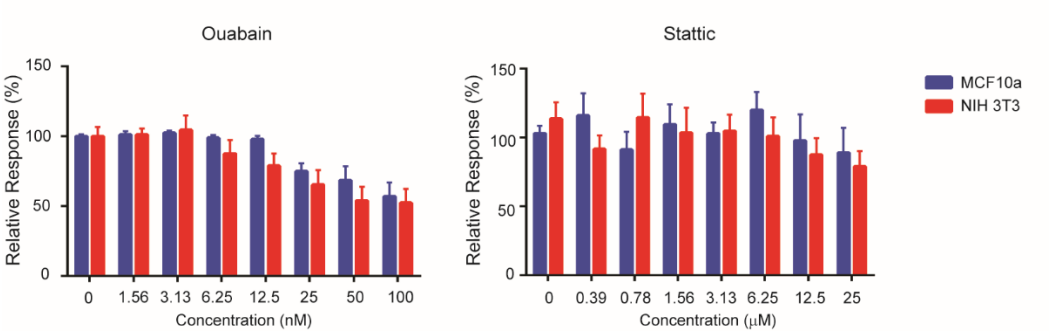

Figure S5. Nrf2 inhibitor cytotoxicity in non-tumorigenic cell lines. Cell viability of MCF10a and NIH 3T3 cells was quantified using the MTT assay after 48 h drug exposure.

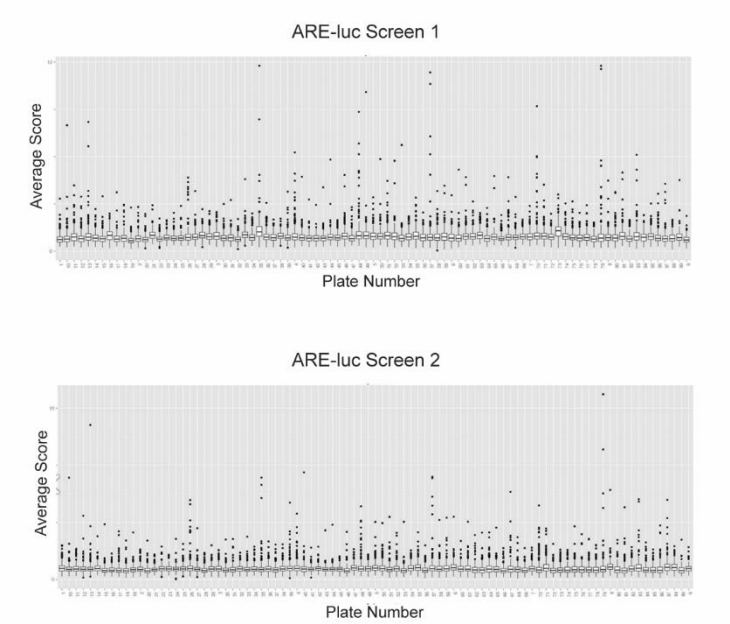

Figure S6. Summary of plate statistics from ARE-luc siRNA screen replicates. Box plots depicting the median, first quantile, third quantile, minimum and maximum normalized scores from each plate of the siRNA library in both screen replicates.

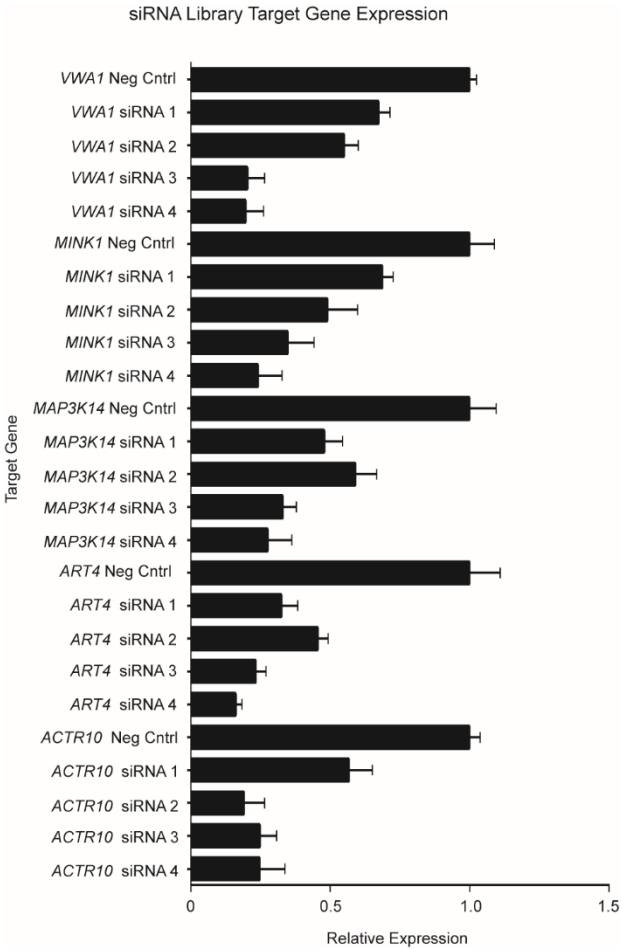

Figure S7. siRNA library target gene expression of selected ARE inhibitor hits. The knockdown efficiency after 48 h treatment of 20 nM concentration of four different non-toxic siRNAs targeting five gene hits from both siRNA ARE inhibitor screens was tested by RT-PCR in the MDA-MB-231 ARE-luc reporter cell line. Gene expression of each target gene is expressed relative to the negative control siRNA treatment.

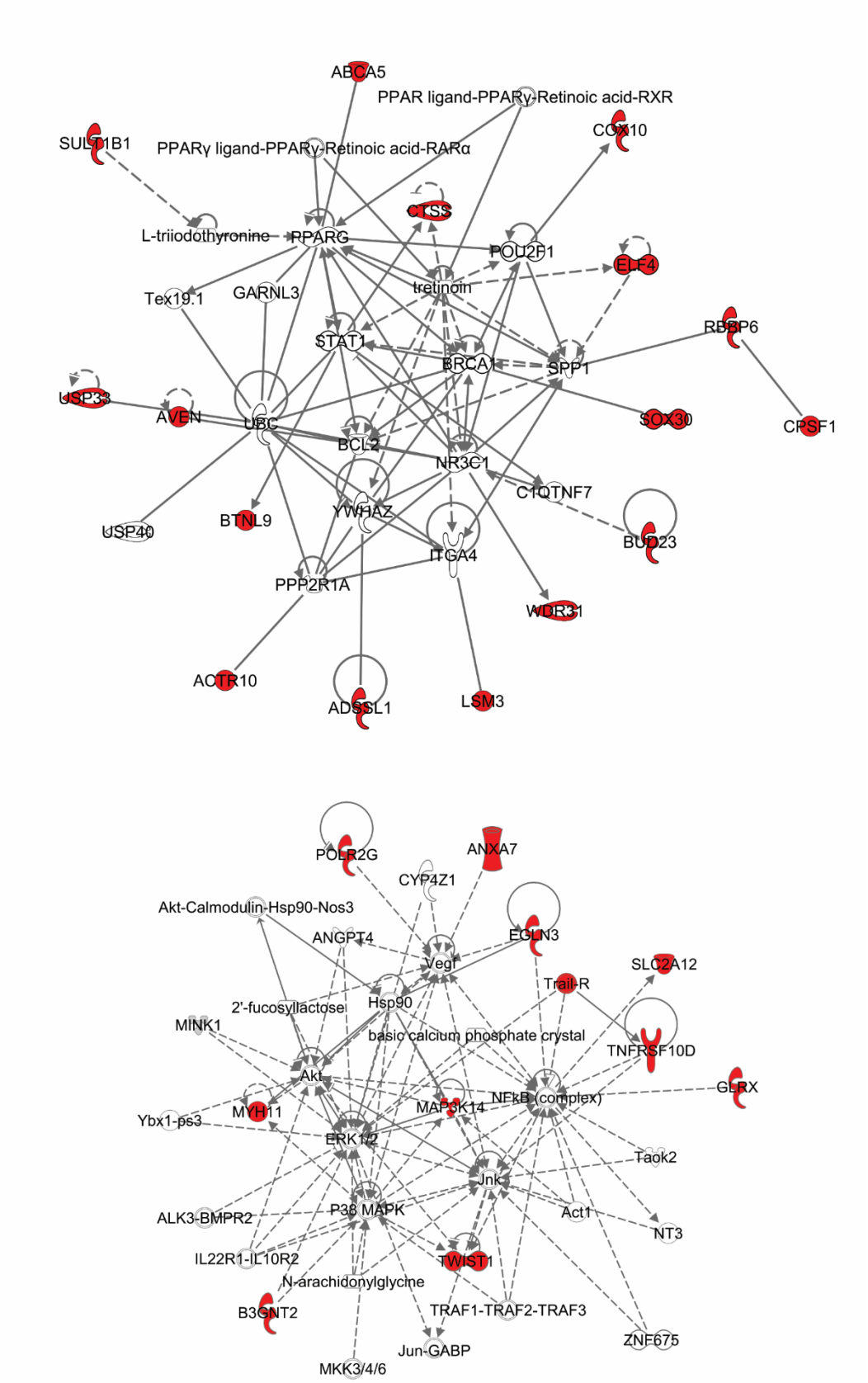

Figure S8. Top two enriched networks containing ARE inhibitor genes hits common to both ARE-luc screen. Red nodes are overlapping hits from both screen replicates.

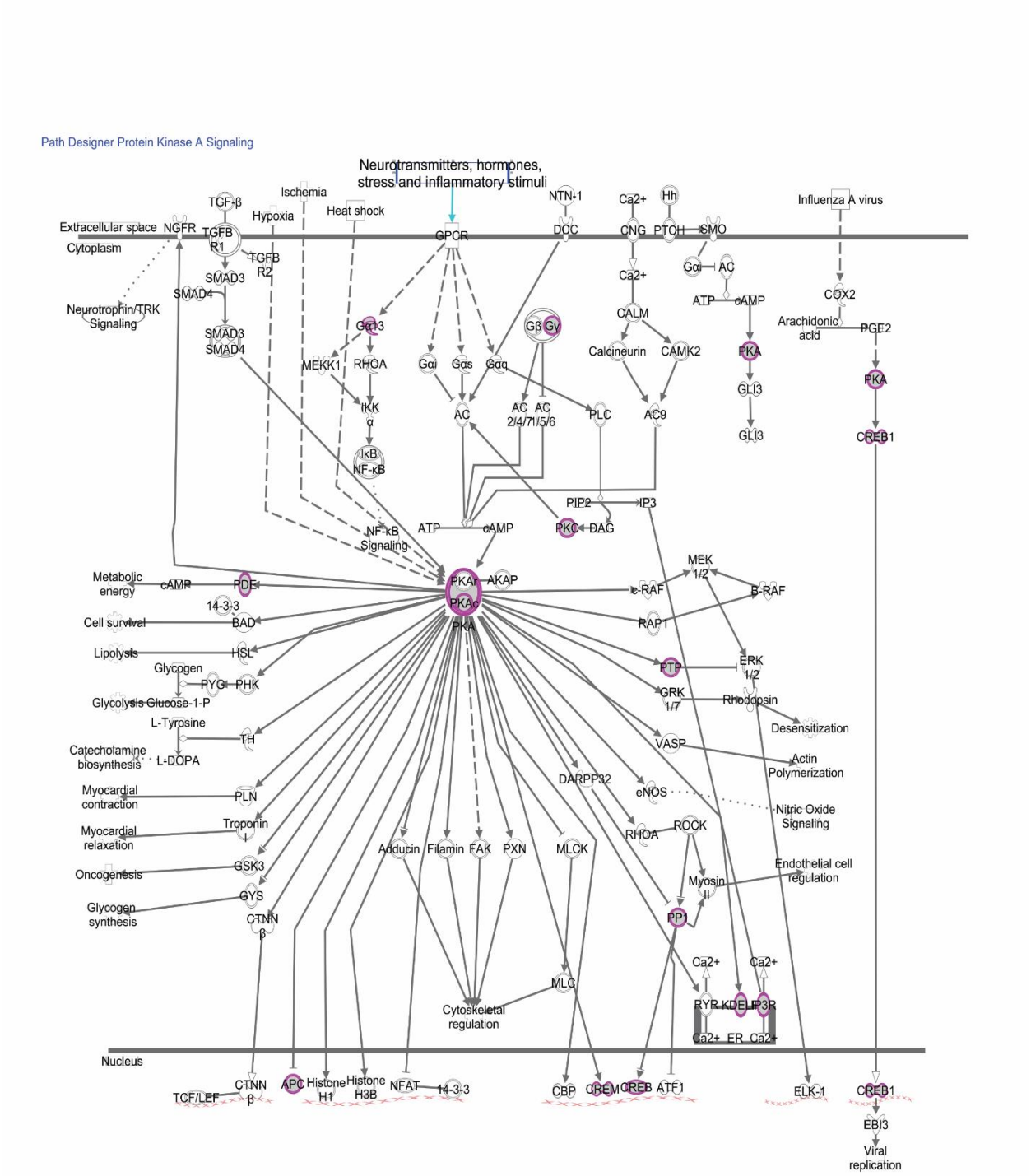

Figure S9. Protein kinase A canonical pathway from Ingenuity Pathway analysis of the combined list of ARE inhibitor gene hits from both ARE-luc siRNA screen. Magenta outlined nodes are the products of the ARE inhibitor gene hits.

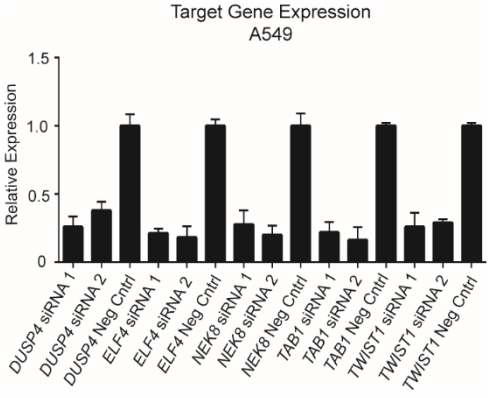

Figure S10. Knockdown efficiency of the two independent siRNAs sourced to confirm the five putative ARE inhibitor gene hits in A549 cells. Quantification of knockdown efficiency was performed by RT-PCR quantification of the expression of each target gene. Target gene expression in response to specific siRNA is expressed relative to its expression in response to the negative control siRNA. *GAPDH* was used as the endogenous control gene.

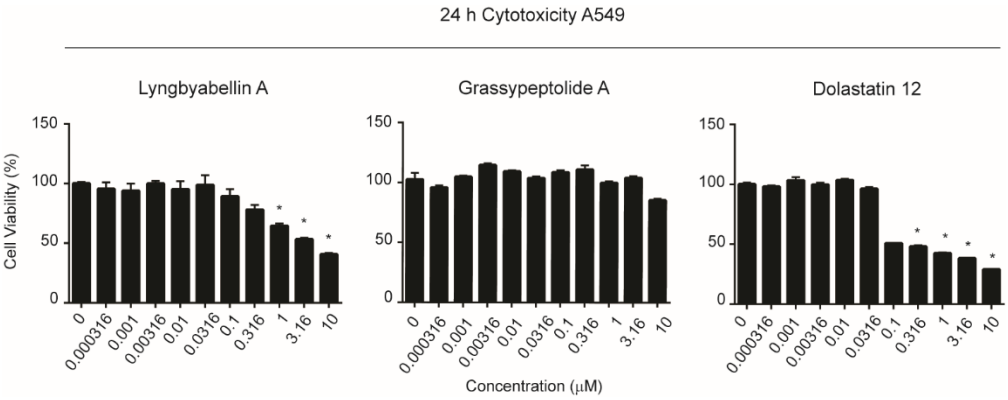

Figure S11. Dose responses of natural product Nrf2 hits lyngbyabellin A, grassypeptolide A and dolastatin 12 on A549 cells after 24 h treatment. Error bars represent ± SEM *P<0.05 relative to vehicle control. Error bars represent ± SEM, * $P \leq 0.05$ (One way ANOVA) relative to negative control.

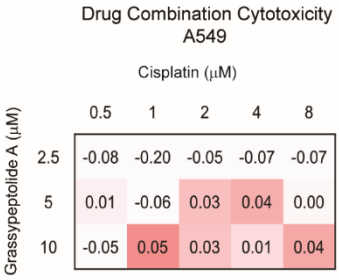

Figure S12. Δ Bliss independence calculations for A549 cells co-treated with grassypeptolide A and cisplatin. A549 cells were treated with grassypeptolide A in serial concentrations for 24 h, followed by treatment with cisplatin in serial concentrations for 24h. Cell viability was quantified using MTT assay.

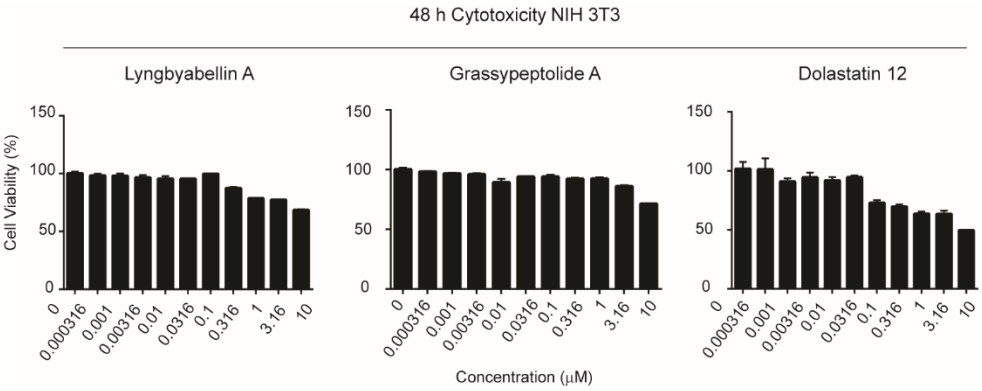

Figure S13. Dose responses of natural product hits lyngbyabellin A, grassypeptolide A and dolastatin 12 on NIH 3T3 cells after 48 h treatment to test cytotoxicity. Error bars represent ± SEM.

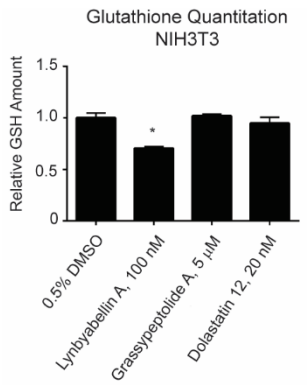

Figure S14. Cellular reduced glutathione (GSH) content level did not increase after 24 h natural product Nrf2 inhibitor hits treatment in NIH 3T3 cells. Error bars represent ± SEM *P < 0.05 (One way ANOVA) relative to vehicle control.

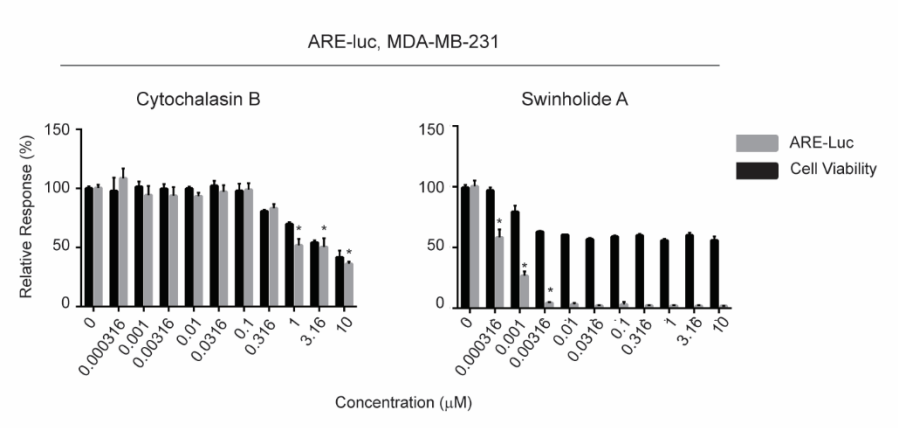

Figure S15. Differential ARE inhibitory effect versus cell viability of cytochalasin B and swinholide A from MDA-MB-231 ARE-luc reporter assay. Error bars represent ± SEM *P < 0.05 (One way ANOVA) relative to vehicle control.

SUPPLEMENTARY TABLES

Table S1: Putative ARE inhibitor from the primary compound screen*

Library	Compound	MAD
SIGMA LOPAC	Emetine dihydrochloride hydrate	-7.9811
SIGMA LOPAC	Sanguinarine chloride	-7.8842
SIGMA LOPAC	Auranofin	-7.8297
SIGMA LOPAC	Stattic	-7.8083
SIGMA LOPAC	Mitoxantrone	-7.5112
SIGMA LOPAC	Icaritin	-7.4364
SIGMA LOPAC	Calcimycin	-7.2965
SIGMA LOPAC	Ouabain	-7.2594
SIGMA LOPAC	Quinacrine dihydrochloride	-7.2167
SIGMA LOPAC	Nestorone	-6.9666
SIGMA LOPAC	ML277	-6.3972
SIGMA LOPAC	Idarubicin	-6.1625
SIGMA LOPAC	Ellipticine	-5.7556
SIGMA LOPAC	Brefeldin A from Penicillium brefeldianum	-5.2709
SIGMA LOPAC	NSC 95397	-5.0709
SIGMA LOPAC	IMS2186	-4.5758
SIGMA LOPAC	ET-18-OCH3	-4.4989
SIGMA LOPAC	Betamethasone	-4.166
SIGMA LOPAC	Tranilast	-4.1219
SIGMA LOPAC	Budesonide	-3.6821
SIGMA LOPAC	AC-93253 iodide	-3.6334
SIGMA LOPAC	ZM 39923 hydrochloride	-3.3938
SIGMA LOPAC	Calmidazolium chloride	-3.3668
SIGMA LOPAC	Dihydroouabain	-3.3332
SIGMA LOPAC	Mevastatin	-3.3038
SIGMA LOPAC	S 24795	-3.1465
SIGMA LOPAC	1,10-Phenanthroline monohydrate	-2.862
SIGMA LOPAC	Bay 11-7085	-2.8096
SIGMA LOPAC	Venlafaxine hydrochloride	-2.7824
SIGMA LOPAC	BPTES	-2.5803
SIGMA LOPAC	NS5806	-2.4695
SIGMA LOPAC	Tegafur	-2.4317
SIGMA LOPAC	Beclomethasone	-2.4173
SIGMA LOPAC	Diphenyleneiodonium chloride	-2.4153
SIGMA LOPAC	Triamcinolone	-2.2672
SIGMA LOPAC	Idazoxan hydrochloride	-2.095
SIGMA LOPAC	Hydrocortisone	-2.0942
SIGMA LOPAC	JNJ-40418677	-2.0691

SIGMA LOPAC	Aminopterin	-2.0288
SIGMA LOPAC	NBQX disodium	-2.0204
SIGMA LOPAC	PAC-1	-2.0138
Spectrum Collection	Homidium bromide	-6.6373
Spectrum Collection	Acrisorcin	-6.0934
Spectrum Collection	Acriflavinium hydrochloride	-5.8926
Spectrum Collection	Dalbergione	-5.8696
Spectrum Collection	Ethacridine lactate	-5.8634
Spectrum Collection	Tetrachloroisophthalonitrile	-5.7489
Spectrum Collection	Captan	-5.5358
Spectrum Collection	Pyrromycin	-5.5164
Spectrum Collection	Phenylmercuric acetate	-5.51
Spectrum Collection	Mitoxantrone hydrochloride	-5.4272
Spectrum Collection	Pyrithione zinc	-5.423
Spectrum Collection	Emetine	-5.4178
Spectrum Collection	Anisomycin	-5.4089
Spectrum Collection	Ouabain	-5.4069
Spectrum Collection	Trisodium ethylenediamine tetracetate	-5.3901
Spectrum Collection	Lanatoside C	-5.3753
Spectrum Collection	Anthothecol	-5.3664
Spectrum Collection	Plumbagin	-5.3601
Spectrum Collection	2,6-dimethoxyquinone	-5.3372
Spectrum Collection	Dihydrocelastryl diacetate	-5.3368
Spectrum Collection	Piplartine	-5.3023
Spectrum Collection	Peruvoside	-5.301
Spectrum Collection	Cycloheximide	-5.2867
Spectrum Collection	Tyrothricin	-5.28
Spectrum Collection	Celastrol	-5.2
Spectrum Collection	Fludarabine phosphate	-5.1858
Spectrum Collection	Tilorone	-5.1557
Spectrum Collection	Thimerosal	-5.1423
Spectrum Collection	Daunorubicin	-5.1394
Spectrum Collection	Convallatoxin	-5.1155
Spectrum Collection	Sanguinarine sulfate	-5.0991
Spectrum Collection	Conessine	-5.0829
Spectrum Collection	Aminacrine	-5.0571
Spectrum Collection	Digitoxin	-5.0332
Spectrum Collection	Tomatine	-5.0087
Spectrum Collection	Epirubicin hydrochloride	-4.9858
Spectrum Collection	Dalbergione, 4-methoxy-4'-hydroxy-	-4.9696
Spectrum Collection	Strophanthidinic acid lactone acetate	-4.9657

Spectrum Collection	Digoxin	-4.9344
Spectrum Collection	Patulin	-4.9014
Spectrum Collection	Dactinomycin	-4.8808
Spectrum Collection	Doxorubicin	-4.8361
Spectrum Collection	Proscillaridin	-4.8358
Spectrum Collection	Pararosaniline pamoate	-4.7859
Spectrum Collection	Quinacrine hydrochloride	-4.7031
Spectrum Collection	Acetaminophen	-4.6982
Spectrum Collection	Acetazolamide	-4.5849
Spectrum Collection	Gentian violet	-4.4782
Spectrum Collection	Digitonin	-4.4304
Spectrum Collection	Dyphylline	-4.4238
Spectrum Collection	Topotecan hydrochloride	-4.3823
Spectrum Collection	Strophanthidin	-4.3146
Spectrum Collection	Niclosamide	-3.9662
Spectrum Collection	Gramicidin	-3.941
Spectrum Collection	Mycophenolic acid	-3.8425
Spectrum Collection	Spermine	-3.3916
Spectrum Collection	Pyrvinium pamoate	-3.3426
Spectrum Collection	Dichlorisone acetate	-3.2974
Spectrum Collection	Tioconazole	-3.1691
Spectrum Collection	Perhexiline maleate	-3.1655
Spectrum Collection	Valinomycin	-3.1373
Spectrum Collection	Cetylpyridinium chloride	-3.1025
Spectrum Collection	Budesonide	-2.915
Spectrum Collection	Flumethasone	-2.8862
Spectrum Collection	Flunisolide	-2.8503
Spectrum Collection	3,4-dimethoxydalbergione	-2.706
Spectrum Collection	Atorvastatin calcium	-2.6821
Spectrum Collection	Benfluorex hydrochloride	-2.6474
Spectrum Collection	Hydrocortisone	-2.5827
Spectrum Collection	Halcinonide	-2.5796
Spectrum Collection	Dexamethasone	-2.5574
Spectrum Collection	Thiram	-2.5337
Spectrum Collection	Atomoxetine hydrochloride	-2.4895
Spectrum Collection	Fluocinolone acetonide	-2.4725
Spectrum Collection	Beta-propiolactone	-2.4687
Spectrum Collection	Mevastatin	-2.4272
Spectrum Collection	2,5-di-t-butyl-4-hydroxyanisole	-2.4164
Spectrum Collection	Dexamethasone acetate	-2.4008
Spectrum Collection	Fluorometholone	-2.3969

Spectrum Collection	Mefloquine	-2.3925
Spectrum Collection	Amcinonide	-2.3685
Spectrum Collection	Physostigmine salicylate	-2.3644
Spectrum Collection	Folic acid	-2.3593
Spectrum Collection	Simvastatin	-2.3292
Spectrum Collection	Hydrocortisone phosphate triethylamine	-2.3202
Spectrum Collection	Betamethasone	-2.3037
Spectrum Collection	Penfluridol	-2.2994
Spectrum Collection	Prednisolone acetate	-2.282
Spectrum Collection	Benzalkonium chloride	-2.2772
Spectrum Collection	Nalbuphine hydrochloride	-2.2688
Spectrum Collection	Digoxigenin	-2.2648
Spectrum Collection	Fludrocortisone acetate	-2.2627
Spectrum Collection	Beclomethasone dipropionate	-2.231
Spectrum Collection	Metoclopramide hydrochloride	-2.2151
Spectrum Collection	Azacitidine	-2.1443
Spectrum Collection	Methylprednisolone sodium succinate	-2.1435
Spectrum Collection	Triclosan	-2.141
Spectrum Collection	Prednisolone	-2.1398
Spectrum Collection	2',4-dihydroxychalcone	-2.1265
Spectrum Collection	Desoxymetasone	-2.1226
Spectrum Collection	Ethacrynic acid	-2.12
Spectrum Collection	Hydrocortisone hemisuccinate	-2.1037
Spectrum Collection	Prednisolone hemisuccinate	-2.0914
Spectrum Collection	Donepezil hydrochloride	-2.0806
Spectrum Collection	Deoxysappanone b 7,3'-dimethyl ether acetate	-2.071
Spectrum Collection	Betamethasone acetate	-2.0663
Spectrum Collection	Hydrocortisone valerate	-2.0539
Spectrum Collection	Cycloserine	-2.0425
Spectrum Collection	Chloranil	-2.0323
Spectrum Collection	Chlorhexidine	-2.025
Spectrum Collection	Tamoxifen citrate	-2.0173
Spectrum Collection	Dexamethasone sodium phosphate	-2.0014

*An inhibitor is defined as one with MAD $\leq$ -2.

Table S2: Putative ARE activators from the primary compound screen*

Library	Compound	MAD Score
SIGMA LOPAC	Iodoacetamide	16.70675
SIGMA LOPAC	Epalrestat	13.90751
SIGMA LOPAC	Kenpaullone	9.287212
SIGMA LOPAC	Aurothioglucose	9.052805
SIGMA LOPAC	Caffeic acid phenethyl ester	8.537189
SIGMA LOPAC	3,4-Dichloroisocoumarin	7.600652
SIGMA LOPAC	CGS-15943	6.114887
SIGMA LOPAC	Ammonium pyrrolidinedithiocarbamate	5.339249
SIGMA LOPAC	DFU	5.197141
SIGMA LOPAC	BMS-195614	4.647482
SIGMA LOPAC	Spermidine trihydrochloride	4.592701
SIGMA LOPAC	Parthenolide	4.484271
SIGMA LOPAC	Nordihydroguaiaretic acid from Larrea divaricata	4.437546
SIGMA LOPAC	BTO-1	4.186073
SIGMA LOPAC	(-)-Eseroline fumarate	3.994886
SIGMA LOPAC	2,3-Dimethoxy-1,4-naphthoquinone	3.775728
SIGMA LOPAC	Auraptene	3.768909
SIGMA LOPAC	Amlexanox	3.640288
SIGMA LOPAC	Pifithrin-mu	3.60019
SIGMA LOPAC	Podophyllotoxin	3.596994
SIGMA LOPAC	Piceatannol	3.590388
SIGMA LOPAC	Dilazep hydrochloride	3.213212
SIGMA LOPAC	Apigenin	3.18705
SIGMA LOPAC	Efavirenz	3.115108
SIGMA LOPAC	Carmustine	3.084224
SIGMA LOPAC	beta-Lapachone	3.068624
SIGMA LOPAC	Lometrexol hydrate	2.997996
SIGMA LOPAC	CPNQ	2.847878
SIGMA LOPAC	N-Methylhistaprodifen dioxalate salt	2.809077
SIGMA LOPAC	Pyrocatechol	2.804935
SIGMA LOPAC	Taurine	2.792656
SIGMA LOPAC	SU 5416	2.562418
SIGMA LOPAC	U0126	2.554656
Spectrum Collection	3,4'-Dimethoxyflavone	18.7509
Spectrum Collection	5alpha-Androstan-3,17-dione	17.2428
Spectrum Collection	Mucic acid	15.24338
Spectrum Collection	Oxyphenbutazone	12.82796
Spectrum Collection	Antiarol	12.37636
Spectrum Collection	Gambogic acid	8.120025

Spectrum Collection	Curcumin	7.281962
Spectrum Collection	Menadione	6.600058
Spectrum Collection	Trichlorfon	6.370996
Spectrum Collection	Arsenic trioxide	6.108303
Spectrum Collection	Phenethyl caffeate (cape)	5.76877
Spectrum Collection	4'-hydroxychalcone	5.601457
Spectrum Collection	Nifuroxazide	4.792062
Spectrum Collection	Phytol	4.508608
Spectrum Collection	Acetyl isogambogic acid	4.405984
Spectrum Collection	Deacetylgedunin	3.942026
Spectrum Collection	Apiin	3.779035
Spectrum Collection	Carbidopa	3.758125
Spectrum Collection	3-Methoxycatechol	3.622134
Spectrum Collection	Lapachol	3.548714
Spectrum Collection	Dihydrojasmonic acid	3.46585
Spectrum Collection	21-Acetoxypregnenolone	3.442577
Spectrum Collection	Pachyrrhizin	3.41852
Spectrum Collection	Picrotin	3.339497
Spectrum Collection	Mundoserone	3.184655
Spectrum Collection	Cryptotanshinone	3.083846
Spectrum Collection	Trichlormethiazide	2.980588
Spectrum Collection	Apomorphine hydrochloride	2.901622
Spectrum Collection	Idebenone	2.889746
Spectrum Collection	Erythromycin stearate	2.888357
Spectrum Collection	6,7-Dichloro-3-hydroxy-2-quinoxalinecarboxylic acid	2.863373
Spectrum Collection	Exemestane	2.800535
Spectrum Collection	Edaravone	2.77155
Spectrum Collection	Juglone	2.727448
Spectrum Collection	Tranilast	2.705352
Spectrum Collection	Chlorthalidone	2.697586
Spectrum Collection	2',4'-Dihydroxychalcone	2.64389
Spectrum Collection	Chlorzoxazone	2.634592
Spectrum Collection	4'-Methoxychalcone	2.628301
Spectrum Collection	Omega-3-acid esters (epa shown)	2.615434
Spectrum Collection	Ethoxzolamide	2.609658

*An inhibitor is defined as one with MAD ≥ -2.5.

Table S3: Enriched networks containing gene hits in common between the two siRNA inhibitor ARE-luc screen replicates*

Network Number	Score	Focus Molecules	Molecules in Network
1	49	28	*AKR1B10*, Ampa Receptor, *APOF*, *ATP6V1E1*, *BOK*, caspase, *COPB1*, *CPSF1*, *CTBP2*, *CYCS*, *EGLN3*, *GLRX*, *GRIA3*, *GUCY1A2*, *HDL*, *HELZ2*, Histone h4, *ITPR3*, *MVD*, *Nos*, *NPR2*, *ORC4*, *PI3K* (family*)*, *Pkc(*s), *RBBP6*, *RBP4*, *SAE1*, *SATB1*, *SEMA4F*, *SLC18A3*, *SNTA1*, *SOX13*, *SPHK1*, *UBE2V2*, *XRCC6*
2	40	25	*ADORA2A*, *ANGPTL2*, ATPase, Collagen(s*)*, *CST1*, *CTSS*, *DDX39A*, *DNA2*, *DUB*, *EIF4A2*, *EPHX4*, *FOXN2*, *KIF20B*, *LSM3*, *MEOX2*, *MID1*, Mmp, *MPG*, NFkB (complex), *PAN2*, *PAX1*, Pro-inflammatory Cytokine, Relaxin, *RPA*, *SERPINA3*, *SLC15A2*, *SLC2A12*, snRNP, *SNRNP40*, *SNRPD1*, *SNRPF*, *SRSF6*, *TRIM35*, Vegf, *VEZF1*
3	39	24	*Akt*, *ALDH7A1*, *ANAPC10*, *CAD*, *CARD6*, *CARD11*, *E3 RING*, Gm-csf, *GNA13*, *GNAZ*, *GNG3*, *GNG4*, I kappa b kinase, Ikb, IKK (complex), Ikk (family), *MAP3K3*, *MAP3K14*, *MEKK3/NIK*, *MOB4*, *NEK8*, NFkB (family), *PKN3*, *PPIA*, *PRDX4*, *RGS8*, *RIPK1*, Sapk, *SMARCD3*, *TAB1*, *TNFRSF1A*, Ubiquitin, *UBR2*, *XIAP*, *ZFPM2*
4	37	23	Alp, Ap1, *ARID3B*, *ATF3*, *CHM*, *CPEB2*, *CTDSP1*, *DNMT3L*, *ELF4*, *ESPN*, *F Actin*, *IFN Beta*, *IFNAR1*, Keratin, *KRT34*, *KRT79*, *KRT85*, *LDL*, *MPP1*, *MYH11*, NADPH oxidase, *NPHS2*, *p70 S6k*, Pdgf (complex), *PGD*, PI3K (complex), *PITPNM1*, *PRKCD*, *PRKD2*, *RAB3A*, *RUNX3*, *SEC23IP*, Smad, Tgf beta, *TWIST1*
5	32	21	BCR (complex), *CD36*, *CUL9*, *CYP4F2*, *EPOR*, *FCGR2A*, *FCRL3*, *GGA3*, *GLMN*, *GST*, *GSTA2*, GTPase, *HBE1*, Ifn, *IgG*, *IL23*, IL12 (family), Immunoglobulin, *IRF4*, Jnk, *LBR*, *MED1*, *MGST3*, NFAT (complex), *PLXNB3*, Rar, *RORC*, Rxr, *SEPHS1*, *STAT5a/b*, *SWAP70*, *SYK/ZAP*, *TBCB*, *TNFRSF10D*, *TYMP*
6	28	19	14-3-3, *ACTA2*, *ADCY*, *BAIAP2*, Cg, Collagen Alpha1, Creb, *CREM*, *DUSP2*, *DUSP4*, *ERK1/2*, *FASTK*, *FSH*, *HAS2*, *HMGA2*, *KIF13B*, *KSR1*, Lh, *MAP2K1/2*, Mek, *MIXL1*, *Myosin*, *NF1*, *PDGF-AA*, Pka catalytic subunit, *PLAT*, *POLR3G*, *PRKACG*, PTPase, *PTPRB*, Raf, *RRM1*, Smad2/3, *SMURF2*, *SRD5A2*
7	27	19	*ADRA1D*, *ANXA7*, *ATP4A*, *C2*, *CACNA1A*, *CALCRL*, Calmodulin, *COX10*, *COX7C*, cytochrome-c oxidase, Focal adhesion kinase, Gpcr, *GPR37*, *GPR152*, *GPR182*, *IL1*, *ILK*, Integrin, *KLHL1*, *LPAR3*, *MAS1L*, *NMDA Receptor*, *NRP1*, *P2RY10*, *P2RY13*, *P38 MAPK*, Pdgfr, Pka, *PLC*, Rac, Ras, Ras homolog, SRC (family), *TCR*, *TIAL1*

8	26	19	*ABCA5*, *AKR1C1/AKR1C2*, *ALDH3A1*, *AMPK*, *ARG2*, *BAX*, Cofilin, Collagen type I, Cyclin A, Cyclin D, Cyclin E, E2f, *ERK*, hexokinase, *KCNH1*, *MYBL2*, *NR4A1*, *OGG1*, Pde, *PDE12*, *PDE4A*, *PDGF BB*, *PGAM2*, *PLOD2*, *PP1/PP2A*, *PP2A*, *PPP1R3C*, *PPP1R3D*, Ppp2c, *PPP2R2A*, *PRKAA*, Rb, *SLC22A4*, *SNAPC3*, *SPSB1*
9	24	18	26s Proteasome, *ACTB*, Actin, *BRCA2*, *BUD23*, Cbp/p300, *CD3*, *CDK1*, *CHD3*, *CK1*, *Ck2*, *CREB1*, Cyclin B, *CYP8B1*, DNA-directed RNA polymerase, *EN1*, *ESPL1*, estrogen receptor, *FOXO1*, *GPX2*, Hdac, *HISTONE*, Histone h3, Hsp70, Hsp90, Mapk, *POLN*, *POLR1A*, *POLR2F*, *POLR2G*, *RAD51C*, RNA polymerase II, *SMARCA1*, *TCF*, *ZNF219*
10	20	15	*ABCE1*, *ADSS*, *ADSSL1*, *ALOX12B*, *ARFGAP2*, *BRCA1*, *CUL3*, *DDX1*, *DNPH1*, *DPAGT1*, *DYNC1H1*, *GALK1*, *HIST2H2BF*, *HM13*, *LYPLAL1*, *MSH4*, *MSH5*, *NBEA*, *NSDHL*, *PDXK*, *PISD*, *PREB*, *PTBP2*, *PYCR3*, *SCLT1*, *STAU1*, *SUCLG2*, *TINCR*, *TMEM17*, *TSN*, *Ube3*, *USP33*, *VCP*, *YWHAZ*, *ZDHHC5*
11	19	15	*AGXT*, *APP*, *ART4*, *BMI1*, *BTBD11*, *CNDP1*, *ECI1*, *ECI2*, *FPR2*, *GALE*, *GPR3*, *GPR12*, *GPR15*, *GPR61*, *GPR78*, *GPT2*, *HRAS*, *HSDL1*, *KCNAB1*, *KIFC1*, *LPAR3*, *MOB3A*, *NLN*, *ORMDL1*, *PHYHD1*, *PITRM1*, *PTBP3*, *RACK1*, *RGL1*, *RXFP3*, *SLC9A9*, *SPON1*, *TOX2*, *ZNF740*, *ZNF385B*
12	18	14	*AGPAT1*, *ANXA10*, *APOBEC3C*, *APTX*, *AVEN*, *BAG3*, *C1QTNF7*, cAMP-Gef, cortodoxone, *CPNE1*, *DIMT1*, *FAM118A*, *FANCC*, *FN1*, *FOCAD*, *GALE*, *IKBKB*, *MINK1*, *NAA20*, *NETO1*, *NR3C1*, *PAX3*, *PCLO*, *POP4*, *PRRG2*, *RBM4*, *RPL10*, *RPP40*, *SDCBP*, *ST8SIA2*, *SULT1B1*, *TEKT1*, *USP1*, *VCL*, *WDR31*
13	17	13	*ACER1*, *ADAM11*, *ADAM18*, *ADAM20*, *ADAM29*, *ADAMTS6*, *ADAMTS8*, *AGPAT2*, *ATF6*, *AURKA*, *BCL2L13*, *EGFR*, *GCNT1*, Interferon alpha, *IVD*, *KIRREL3*, *LILRA4*, *MBOAT2*, *MBTPS*, *MBTPS2*, Metalloprotease, *MYH16*, *NDUFS4*, *NINJ2*, *NNMT*, *PPARG*, *RILP*, *SOD2*, *SOX8*, *SOX30*, *SPP1*, *STK11*, *SWT1*, *TDRD7*, *TGFB1*
14	15	13	*ADAT1*, *AGT*, *AMACR*, *ANXA9*, *BARHL1*, *BNC1*, *BTNL9*, *C5orf22*, *CA6*, *CCDC25*, *CH25H*, *COX8A*, *CYP4F3*, *FGF13*, Gsk3, *HIF3A*, *HMGN4*, *HNF4A*, *ITIH4*, *MED7*, *MGST2*, *MOCS3*, *MTHFS*, *OSM*, *PEMT*, *RNASE4*, *SAA2*, *SLC25A32*, *SLC4A3*, *SQOR*, *STAT1*, Stat1-Stat3, *SUCLA2*, *VEGFA*, *ZAN*
15	15	12	*ACSL6*, *ADGRG6*, *APOBEC3B*, *ATP11B*, *ATP8A1*, *B3GNT2*, *B3GNT4*, *B3GNT7*, *B4GALNT1*, *BTLA*, *CD3*,

			CD3 group, *COMP*, *CXCR6*, *DPEP2*, *FFAR1*, *GPR35*, *GPR84*, *GPR176*, *IL21R*, *ITGA10*, *ITGAV*, *KCNK3*, *KDELR2*, *LOXL3*, N-acetyllactosaminide beta-1, 3-N-acetylglucosaminyltransferase, *NFAM1*, *PCSK9*, *PDPN*, *PRKD1*, *SERPINB10*, *SIT1*, *SYK*, *TNF*, *TPST1*
16	15	12	*ADGRG6*, *ASMT*, beta-estradiol, cyclic AMP, *DDB2*, *FOS*, *FPR3*, *GCG*, *GHRHR*, *GIPR*, *GLP2R*, *GPR39*, *GPR132*, *GPR139*, *GPR173*, *MC5R*, *MCHR1*, *NKX2-1*, *NKX6-2*, *NPY*, *NPY2R*, *PTER*, *RXFP2*, *RXRA*, *S1PR2*, *SLC27A5*, *SLC6A14*, *SUCNR1*, *SULT1A2*, *TAC3*, *TACR2*, *TACR3*, *TIGD3*, *UQCR10*, *XYLT1*
17	12	11	*ANKRD2*, *APH1B*, *Cd64*, *CD79A*, *CHAD*, *CLEC4C*, *COL14A1*, *CPXM1*, *DYRK3*, *EGFL6*, *GCNT2*, heparin, *HIPK1*, Hla-abc, *IDH3B*, *IFNB1*, *INPP4A*, Intersectin, iodine, *KLB*, *LY6G5B*, *MAPK3*, *MIR155HG*, *PEBP4*, phosphatidylinositol-3, 4, 5-triphosphate, *SLC2A8*, *SLC30A4*, *SNTG1*, *SPRR2A*, *TP53*, triiodothyronine, reverse, *TRIM47*, *TRIM67*, *VWA1*, *YES1*
18	2	1	*HELT*, *TADA2A*
19	2	1	*OBP2A*, *OBP2B*
20	1	1	*ACAD11*, *APLP1*, *CNTN5*

*Network enrichment amongst overlapping set of inhibitor gene hits from both siRNA ARE-Luc screen replicates determined by IPA analysis.

Table S4: Canonical pathway enrichment for the combined ARE inhibitor gene hit list from both siRNA ARE-luc screen replicates*

Ingenuity Canonical Pathways	-log (p-value)	Ratio	Molecules
Protein Kinase A Signaling	3.86	0.0443	*GNG4, PDE12, PPP1R3C, PDE4A, ANAPC10, GNG3, DUSP2, PPP1R3D, PTPRB, PRKCD, PRKACG, CREB1, CREM, ITPR3, DUSP4, GNA13, KDELR2*
CREB Signaling in Neurons	3.77	0.0598	*POLR2G, GNG4, POLR2F, PRKCD, PRKACG, CREB1, ITPR3, GNG3, GNA13, GNAZ, GRIA3*
Relaxin Signaling	3.77	0.0649	*GNG4, PDE12, PRKACG, CREB1, GUCY1A2, PDE4A, GNG3, GNA13, GNAZ, NPR2*
Cellular Effects of Sildenafil (Viagra)	3.75	0.0714	*ACTA2, GPR37, ACTB, PRKACG, ITPR3, GUCY1A2, PDE4A, MYH11, CACNA1A*
Dopamine-DARPP32 Feedback in cAMP Signaling	3.63	0.0625	*PPP1R3D, PPP2R2A, PPP1R3C, PRKCD, PRKACG, CREB1, ITPR3, CREM, GUCY1A2, CACNA1A*
Androgen Signaling	3.45	0.0727	*POLR2G, GNG4, POLR2F, PRKCD, PRKACG, GNG3, GNA13, GNAZ*
Induction of Apoptosis by HIV1	3.44	0.1	*MAP3K14, RIPK1, TNFRSF1A, CYCS, BAX, XIAP*
Cardiac β-adrenergic Signaling	3.43	0.0647	*GNG4, PPP1R3D, PPP2R2A, PPP1R3C, PDE12, PRKACG, PDE4A, GNG3, CACNA1A*
IL-1 Signaling	3.2	0.0761	*GNG4, MAP3K14, PRKACG, GNG3, GNA13, GNAZ, TAB1*
Death Receptor Signaling	3.2	0.0761	*MAP3K14, RIPK1, ACTA2, TNFRSF1A, ACTB, CYCS, XIAP*
TNFR1 Signaling	3.03	0.104	*MAP3K14, RIPK1, TNFRSF1A, CYCS, XIAP*
Bile Acid Biosynthesis, Neutral Pathway	3	0.231	*SLC27A5, AKR1C1/AKR1C2, CYP8B1*
Production of Nitric Oxide and Reactive Oxygen Species in Macrophages	2.99	0.0518	*MAP3K14, PPP1R3D, PPP2R2A, APOF, TNFRSF1A, PPP1R3C, PRKCD, ARG2, MAP3K3, RBP4*
Dopamine Degradation	2.92	0.133	*ALDH3A1, SULT1B1, SULT1A2, ALDH7A1*
Fatty Acid β-oxidation I	2.92	0.133	*SLC27A5, ECI2, ACSL6, IVD*

Cardiac Hypertrophy Signaling	2.91	0.0472	*GNG4, MAP3K14, PRKACG, CREB1, GNG3, GNA13, GNAZ, MAP3K3, CACNA1A, TAB1, ADRA1D*
ERK/MAPK Signaling	2.89	0.0503	*ELF4, PPP1R3D, PPP2R2A, PPP1R3C, PRKCD, PRKACG, CREB1, DUSP4, DUSP2, KSR1*
Breast Cancer Regulation by Stathmin1	2.81	0.049	*GNG4, PPP1R3D, PPP2R2A, PPP1R3C, PRKCD, PRKACG, ITPR3, GNG3, GNA13, CDK1*
Corticotropin Releasing Hormone Signaling	2.77	0.0642	*PRKCD, PRKACG, CREB1, ITPR3, NR4A1, GUCY1A2, NPR2*
Synaptic Long Term Depression	2.72	0.0563	*PPP2R2A, PRKCD, ITPR3, GUCY1A2, GNA13, GNAZ, NPR2, GRIA3*
TWEAK Signaling	2.71	0.118	*MAP3K14, RIPK1, CYCS, XIAP*
GPCR-Mediated Nutrient Sensing in Enteroendocrine Cells	2.65	0.0706	*GNG4, PRKCD, PRKACG, ITPR3, GNG3, FFAR1*
Fatty Acid α-oxidation	2.57	0.167	*ALOX12B, ALDH3A1, ALDH7A1*
G Beta Gamma Signaling	2.57	0.0682	*GNG4, PRKCD, PRKACG, GNG3, GNA13, GNAZ*
Synaptic Long Term Potentiation	2.55	0.0588	*PPP1R3D, PPP1R3C, PRKCD, PRKACG, CREB1, ITPR3, GRIA3*
Apoptosis Signaling	2.54	0.0674	*MAP3K14, TNFRSF1A, CYCS, BAX, CDK1, XIAP*
Arginine Degradation VI (Arginase 2 Pathway)	2.45	0.333	*PYCR3, ARG2*
Zymosterol Biosynthesis	2.45	0.333	*NSDHL, LBR*
Xenobiotic Metabolism Signaling	2.37	0.0403	*GSTA2, MAP3K14, PPP2R2A, MED1, PRKCD, MAP3K3, ALDH3A1, MGST3, SULT1B1, SULT1A2, ALDH7A1*
SAPK/JNK Signaling	2.23	0.0583	*MINK1, RIPK1, DUSP4, GNA13, MAP3K3, TAB1*

*Only the top 30 enriched canonical pathways are listed for brevity.